El-Mahllawy and Mohsen
*Beni-Suef Univ J Basic Appl Sci* (2024) 13:57
https://doi.org/10.1186/s43088-024-00517-6

Beni-Suef University Journal of Basic and Applied Sciences

RESEARCH

Open Access

# Characterization and utilization capabilities of industrial wastes for green bricks production

Medhat Sobhy El-Mahllawy[1] and Sarah Akram Mohsen[2*]

## Abstract

**Background** The goal of this study is to develop a feasible and sustainable solution to manage the use of industrial wastes of ground granulated blast-furnace steel slag (GGBS) activated by cement kiln dust (CKD) and quicklime (QL). Using activated GGBS in the manufacture of stabilized green bricks is still uncommon in Egypt in such applications. Five clay-based mixtures, each with varying replacement ratios (5–10, wt.%) of CKD and QL, were studied. Laboratory tests were conducted on cylindrical specimens made from these mixtures, which were left to cure for periods of up to 60 days. The raw materials and lab-made specimens were analyzed using particle size analysis, differential thermal analysis, X-ray fluorescence, and X-ray diffraction techniques. The physical and mechanical properties of the cured specimens were also determined and evaluated according to standard specifications. Furthermore, the durability of the cured specimens was evaluated against collapsibility in water.

**Results** It has been observed that adding QL and CKD to the stabilized green specimens of different mixes can enhance their engineering properties with curing age increasing. This is due to the pozzolanic reaction, which fills the pore structure with calcium silicate hydrates and calcium aluminate hydrates gel. The ratio of QL and CKD used significantly affected the engineering properties of the specimens. The study found that using 20% GGBS and 5% QL led to an increase in compressive strength (266 kg/cm$^2$) at the density of (2.15 g/cm$^3$), while also water absorption was reduced (8%) to give superior results. When GGBS and CKD were combined, a higher content of CKD (10 wt.%) gave better results compared to (5 wt.%) CKD. Furthermore, the physical and mechanical properties of the tested specimens (MD 1, MD II, MD III and MD IV) met the acceptable limits of dry compressive strength (30–70 kg/cm$^2$), water absorption (8–15%), and density (1.7–2 gm/cm$^3$), as specified by the Egyptian standard specifications for buildings used compressed earth blocks.

**Conclusion** The CKD and QL act as alkali activators for GGBS and can be utilized in masonry construction.

**Keywords** Cement kiln dust, Ground granulated blast-furnace slag, Quicklime, Stabilized green bricks

## 1 Background

Over 50 million tons of various types of cement were produced annually in Egypt, accompanied by 3 million tons of cement kiln dust (CKD) produced in dry lines. The worldwide generation of CKD is expected to reach approximately 220 million tonnes by 2030 [1]. CKD is an ultra-fine grayish particle formed as a by-product of the cement industry. Nevertheless, the ongoing shift in the cement industry to the dry method increased the accumulated cement kiln dust. In general, the composition of CKDs varies, although most of them contain the minor constituents of quartz, calcium carbonate, and

*Correspondence:
Sarah Akram Mohsen
sarah-akram@alexu.edu.eg
[1] Raw Building Materials and Processing Technology Research Institute, Housing and Building National Research Center (HBRC), 87 El-Tahreer St., P.O. Box 1770, Dokki, Giza, Egypt
[2] Geology Department, Faculty of Science, Alexandria University, 49, Baghdad Street, Moharam Bek, Alexandria, P.O:21511, Egypt

calcium oxide (free lime). When combined with water, the majority of CKDs generate pH levels that are comparatively highly alkaline. These materials are suitable for various applications due to their increased alkalinity, fine particle size, and cementitious characteristics. The major existing applications of these CKDs are for soil stabilization [2–4]. High free lime content in CKDs has been reported to be more successful in increasing strength [5], lowering the swelling potential, and decreasing the plasticity of Na-montmorillonite clay [6].

Nonetheless, there is a need to encourage the long-term use of industrial by-products, such as granulated blast furnace slag (GGBS), in applications of soil stabilization, polluted land restoration, and cement production [7–9]. Molten slag is created at the blast furnace, where iron ore, limestone, and coke are heated to 1500 °C. For GGBS to be effective in stabilizing soil, it must first undergo chemical activation by an alkaline activator due to its low hydration level. The ideal ratio of lime to GGBS is one to four parts of GGBS for full hydration, pozzolanic reactions, and high strength [10]. More GGBS content is predicted to improve durability and prolong curing [11].

On the other hand, some countries, such as China, have banned the production and use of solid fired clay bricks since 2003 due to environmental and economic concerns [12, 13]. In Bangladesh, the government introduced 'The Brick Manufacturing and Brick Kilns Establishment (Control) Act 2013' [14] to manage the negative impacts of brick kilns. This act is considered the primary law in the country for regulating brick manufacturing and the establishment of brick kilns [15]. As the need for sustainable design approaches grows, there is a rising demand for new construction technologies that have minimal environmental impact. One way to achieve this is by increasing the use of supplementary cementitious materials, which can partially or fully replace fired bricks, thus reducing greenhouse gas emissions. Various industrial by-products have been used as raw materials to produce stabilized green bricks. It is fabricated from cementitious material through compaction, solidification, stabilization, and curing without burning and steaming. A range of cementitious materials can produce eco-friendly bricks [16–18].

The objective of this research was to find a practical and long-lasting solution to manage the use of industrial wastes of GGBS activated by CKD and QL of various dosages in clay-based mixes for the manufacture of stabilized green bricks. This research is one of the early efforts made in Egypt to advance the use of this unfired technology in the construction sector. Stabilized green bricks incorporating waste materials provide a sustainable and eco-friendly alternative to traditional masonry bricks.

## 2 Materials and methods

### 2.1 Raw materials

The raw materials used in this study included Kafr Homied clay (KHC), sand, ordinary Portland cement (OPC), ground granulated blast furnace slag (GGBS), cement kiln dust (CKD), and quick lime (QL). The used clay sample was taken six meters below the ground's surface from a clay quarry near Kafr Homied village in the Giza governorate of Egypt, 50 km south of Cairo.

Ordinary Portland cement (OPC) was supplied by the Suez Cement Company, Egypt. It was of the CEM (I) 42.5 type and produced locally in accordance with BS EN [19]. The quicklime was obtained from the Egyptian company for lime. CKD was provided by Helwan Cement Co. (30 km south of Cairo). The GGBS was supplied by the Egyptian Co. for Steel Industries, Helwan, Egypt.

### 2.2 Techniques

The materials used and the stabilized green specimens were characterized using XRD, XRF, and particle size distribution techniques. Furthermore, the mineralogical and hydration products of the investigated mixes at different curing ages were monitored using differential thermal analysis using the thermal analyzer DT 50 (Schimadzu Co., Kyoto, Japan). A digital pH meter was used to measure the pH value at 20°C in accordance with ASTM D4972-19[20].

### 2.3 Mix composition and specimen preparation

To study the effect of the CKD and QL on the engineering properties of the stabilized green bricks, five mixtures, namely MD (Control Mix), MD I, MD II, MD III, and MD IV, were created for the research, as listed in Table 1.

5% of ordinary Portland cement (OPC) was added to accelerate the initial setting time. As a non-plastic material, the sand was used to increase the durability of the final product, reduce the effect of clay shrinkage that may occur, and accelerate the formation of hydration products. Surficial pits were seen in the mixture's coarse quartz grains, which served as a preferred location for CSH nucleation. This clarifies the significance of adding sand for the enlargement of the hydration products [21].

The mixing process of the studied mixes was performed in two stages. In the first stage, all ingredients, except the cement, were shaken manually for at least 2 min while the plastic bag was overturned. Then, the bag was compressed by hand to remove any trapped air inside. The mixing process was continued by mixing the prepared mixture with water (10% water spraying) in a laboratory mixer for a minimum of three minutes after adding water until the mix appeared homogeneous and reached a wetting touch. The mixed materials were kept in a covered

**Table 1** Composition and proportion of the studied mixes, wt. %

| Mix code | Mix ingredient, % | | | | | |
|---|---|---|---|---|---|---|
| | KHC | Sand | OPC | GGBS | CKD | QL |
| MD (Control) | 55 | 15 | 5 | 25 | – | – |
| MD I | 55 | 15 | 5 | 20 | 5 | – |
| MD II | 50 | 15 | 5 | 20 | 10 | – |
| MD III | 55 | 15 | 5 | 20 | – | 5 |
| MD IV | 50 | 15 | 5 | 20 | – | 10 |

bucket for three days. In the second stage, the cement was added and combined with water to achieve suitable consistency. Using a conventional manual compaction apparatus, the mixes under study were formed into small, compacted cylinders of 20 mm in diameter and 40 mm in height, with a compression of 10.0 Mpa.

After the compaction was finished, the specimens were demolded about ten seconds after the compaction was finished. After being labeled, they were kept at 23 °C ± 2 and ≤ 80% ± 2 relative humidity (RH) in a curing stainless box until the testing periods of 7, 14, 28, and 60 days. Five sets of compressed specimens were created in the lab. A covered stainless-steel box was used to minimize the effects of carbon dioxide and carbonation.

### 2.4 Physico-mechanical property tests

Several tests were conducted after reaching the curing period to determine the main engineering characteristics of the manufactured stabilized specimens, including water absorption, bulk density, and compressive strength. The taken specimens from the box were carefully cleaned with a wiping tissue to remove any surface moisture and then dried at 60° C for 24 h before each test. The prepared specimens were tested according to ASTM standards and evaluated according to the Egyptian code for the building by the stabilized and compressed earth soil [22]. To assess the durability of the made specimens in a wet environment by visual observations, specimens of varying mixes and curing ages were completely submerged in tap water for seven days. The results were recorded for each mix at the testing ages of 7, 14, 28, and 60 days.

## 3 Results

### 3.1 Characterization of the raw materials

The results of chemical composition using XRF and the pH value of raw materials (Table 2) revealed that the used QL is classified by the Egyptian Standard Specification [23] as non-fat (lean clay). Also, it was stated that the content of actual free lime (uncombined CaO) is much greater in the QL (95%) than in the CKD (~ 20%), calculated by the XRD analysis [24]. The clay sample's composition matches the common composition of the low-grade clays, and noticeable $SO_3$ and $Na_2O$ contents were observed.

**Table 2** Chemical composition using XRF and the pH value of the used raw materials (wt. %)

| Oxide content | KHC | Sand | OPC | GGBS | CKD | QL |
|---|---|---|---|---|---|---|
| $SiO_2$ | 48.61 | 93.88 | 20.59 | 34.30 | 13.34 | 3.45 |
| $Al_2O_3$ | 22.51 | 3.76 | 4.08 | 11.60 | 3.62 | 2.76 |
| $Fe_2O_3$ | 6.87 | 0.68 | 3.31 | 0.78 | 2.83 | 0.29 |
| CaO | 1.64 | 0.55 | 62.71 | 30.20 | 56.95 | 67.68 |
| MgO | 1.22 | 0.37 | 1.95 | 7.39 | 2.63 | 1.41 |
| $Na_2O$ | 3.11 | 0.21 | 0.18 | 0.94 | 2.26 | 0.09 |
| $K_2O$ | 0.92 | 0.09 | 0.18 | 0.96 | 3.02 | 0.04 |
| $SO_3$ | 3.12 | 0.02 | 2.95 | 3.37 | 3.83 | 0.45 |
| $TiO_2$ | 1.19 | 0.10 | 0.02 | 0.48 | 0.30 | Nil |
| BaO | Nil | Nil | Nil | 5.13 | Nil | Nil |
| MnO | 0.08 | Nil | Nil | 4.56 | Nil | 0.06 |
| LOI | 10.53 | 0.23 | 3.81 | 0.12 | 10.80 | 23.50 |
| $Cl^-$ | 0.86 | Nil | Nil | Nil | 3.52 | Nil |
| pH | 6.5 | 6.7 | 14.0 | 6.1 | 13.2 | 12.4 |

The Egyptian slag is characterized by its higher content of BaO (~5%), MgO (~7%), and MnO (~5%) than the common international standard. The hydraulic activity of the used slag equals 1.43 according to the following formula [$(CaO + MgO + Al_2O_3)$ / $SiO_2$]. In most countries, the formula result should be ≥ 1.0, and in Germany, ≥ 1.4 to predict good hydraulic reactivity of slags or compressive strength of blended materials [25].

The results of the XRD analysis presented in Fig. 1 and Table 3 clarified the mineralogy of the used clay in terms of clay and non-clay minerals. Figure 2 shows the results of the XRD analysis of the OPC, CKD, sand, QL, and GGBS used. GGBS is almost vitreous with an amorphous characteristic hump of the glassy phases between 25°–35° 2$\theta$, but also a minor content of akermanite phase ($Ca_2MgSi_2O_7$) is also detected. This means that the used slag belongs to water-cooled blast furnace slag, which is hydraulically more reactive than air-cooled. In general, the results of the chemical composition match the XRD results.

It was observed that 90% of the particles of KHC, OPC, GGBS, CKD, and QL samples passed through a 63 µm sieve. The cement kiln dust is the finest material, followed by clay, quicklime, cement, and slag, and the last is sand, the coarsest material (Tables 4 and 5).

### 3.2 Chemical analysis of the mixes

The oxide contents, C/S ratios and pH values of the studied mixes are shown in (Table 6). The pH value of the mix MD control (10.1) is attributed to the cement present. The C/S ratio clarifies that mixes the MD III and MD IV that contain the QL content have the highest values (0.49 and 0.55, respectively), followed by mixes MDI and MDII that contain the CKD contents (0.35 and 0.37, respectively), then the mix MD control (control mix) that contains no activators with a C/S value of 0.28.

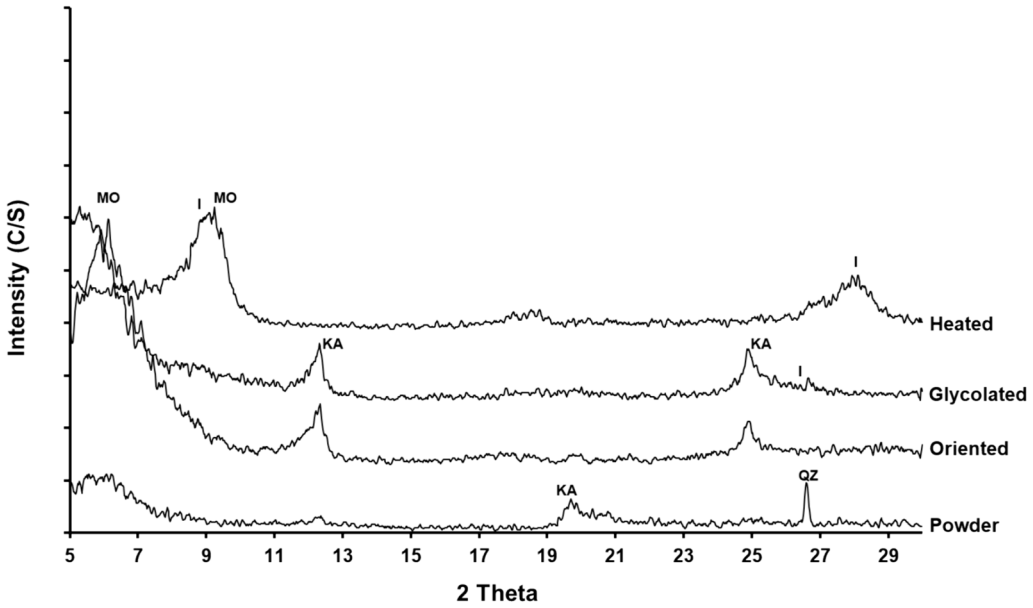


**Fig. 1** XRD patterns of the bulk clay sample (powder), heated, glycolated, and oriented of KHC fraction (MO: Montmorillonite, I: Illite, KA: Kaolinite, QZ: Quartz)

**Table 3** Mineralogical composition of Kafr Homeid bulk clay (KHC) sample and its semi-quantitative minerals (%)

| Mineral | | Chemical formula | (Semi-quantitative percentage) |
|---|---|---|---|
| Montmorillonite | Clay mineral | $(Na, Ca)_{0.3}(Al, Mg)_2Si_4O_{10}(OH)_2 \cdot n\ (H_2O)$ | 57 |
| Kaolinite | Clay mineral | $Al_2Si_2O_5\ (OH)_4$ | 23 |
| Illite | Clay mineral | $(K, H_3O)(Al,Mg,Fe)_2(Si,Al)_4O_{10}[(OH)_2,(H_2O)]$ | 5 |
| Quartz | Non-clay mineral | $SiO_2$ | 7 |
| Feldspar | Non-clay mineral | $CaAlSi_3O_8$ | 2 |
| Gypsum | Non-clay mineral | $CaSO_4$ | 5 |

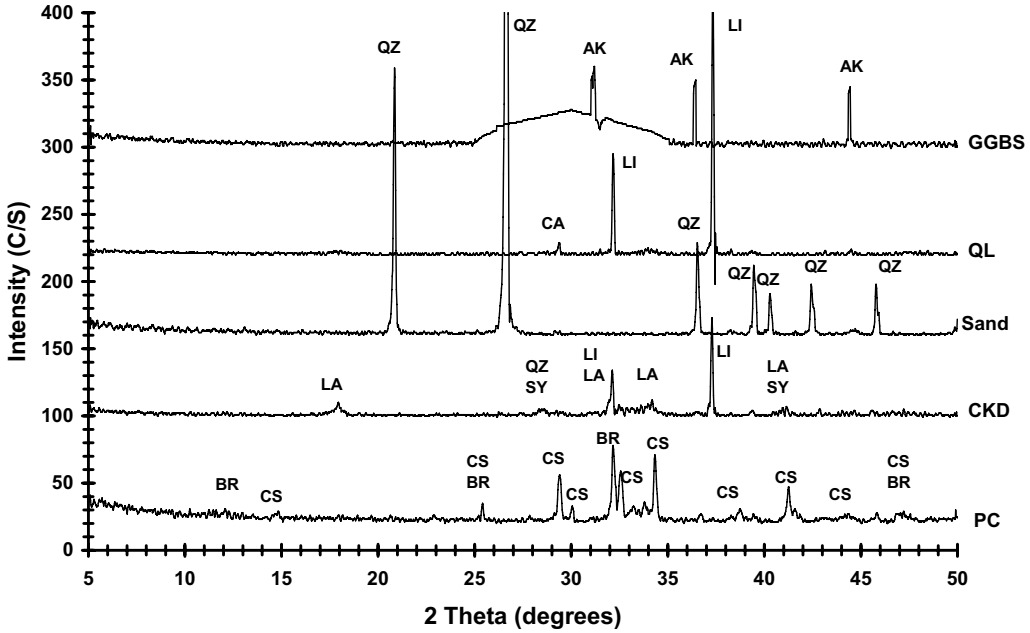


**Fig. 2** XRD patterns of the used materials (QZ: Quartz, AK: Akermanite, LI: Lime, CA: Calcite, LA: Larnite, SY: Sylvite, BR: Brownmillerite, CS: Calcium silicate)

**Table 4** Particle size distribution of the used sand by laser diffraction analyzer

| Particle size (μm) | Sand (%) |
|---|---|
| > 1700 | 0.43 |
| 1000–1700 | 12.91 |
| 500–1000 | 59.37 |
| 250–500 | 25.58 |
| 125–250 | 1.71 |
| 63–125 | Nil |
| Mean size (μm) | 701.51 |
| Distribution type | Unimodal |

### 3.3 X-ray diffraction analysis of the mixes

As shown in Fig. 3, the examined specimens of the mix MD control (without activators) at seven days were found to contain phases of akermanite, quartz, gypsum, kaolinite, and montmorillonite. Accompanied by increasing the curing times from 28 up to 60 days, the hydration products of cementitious character (CSH and CASH) are developed and exhibited as weak reflections due to the poor degree of crystallization. The presence of the montmorillonite phase means that the clay minerals are not shared in forming cementitious phases. The XRD patterns of specimens of the mixes MD I (5wt.% CKD) and MD II (10wt.% CKD) show ettringite and gypsum (Figs. 4, 5) at the early stage of curing age (7 days) due to the presence of high content of sulfate (2.21–3.67%, respectively) but with the progressing of curing age it was consumed. Also, it was noticed that as the curing age increased, the hydration products of calcium silicate hydrates (CSH) and calcium aluminosilicate hydrates (CASH) increased. The calcium silicate hydrates are poorly crystallized and give only weak XRD intensity.

Moreover, it was observed that the formed hydration products were developed and affected the crystallinity of quartz, akermanite, and kaolinite minerals. The peak intensity of the hydration products in the specimens of MD III and MD IV (Figs. 6, 7) are longer than those of the MD I and MD II mixes. Also, it was found that the portlandite phase was only present in the patterns of the mix MD IV (10% QL, Fig. 7), associated with peak intensity increasing with the curing age. This is attributed to the excess of free CaO in the mix, particularly at 60 days of curing.

### 3.4 Differential thermal analysis of the mixes

According to [26], the DTA analysis was interpreted as follows: The endothermic peaks occurring in the temperature range around 80°–90 °C and 130°–140 °C (single peak) are due to the loss of hygroscopic water and stepwise removal of water in a low concentration gypsum, respectively. The single or dual small peaks in some curves occurred at the temperature range 240°–320 °C, representing dehydration reactions involving

**Table 5** Particle size distribution of KHC, OPC, GGBS, CKD, and QL as measured by laser diffraction analyzer

| Grain size (μm) | KHC (%) | OPC (%) | GGBS (%) | CKD (%) | QL (%) |
|---|---|---|---|---|---|
| > 210 | 0.06 | 0.13 | 0.00 | 0.00 | 0.00 |
| 210–125 | 1.59 | 3.37 | 0.47 | 0.00 | 0.00 |
| 125–63 | 2.21 | 11.38 | 7.87 | 0.00 | 0.00 |
| 63–32 | 3.12 | 17.71 | 28.67 | 0.00 | 0.31 |
| 32–16 | 8.33 | 20.16 | 30.57 | 0.00 | 7.07 |
| 16–8 | 32.07 | 29.61 | 19.46 | 0.00 | 26.58 |
| 8–4 | 33.42 | 14.23 | 7.07 | 12.56 | 27.32 |
| 4–1 | 18.71 | 3.41 | 4.22 | 85.82 | 32.91 |
| < 1 | 0.49 | 0.0 | 1.67 | 1.62 | 5.81 |
| Mean size (μm) | 13.58 | 32.34 | 29.19 | 2.48 | 6.76 |
| Distribution type (not presented) | Unimodal (right-skewed) | Bimodal | Unimodal (left-skewed) | unimodal | Unimodal (left-skewed) |

**Table 6** Chemical composition, C/S ratio, and pH value of the studied mixes wt.%

| Oxide content % | MD control | MD I | MD II | MD III | MD IV |
|---|---|---|---|---|---|
| $SiO_2$ | 40.26 | 44.45 | 45.09 | 41.14 | 42.38 |
| $Al_2O_3$ | 17.15 | 15.88 | 15.75 | 13.23 | 11.78 |
| $Fe_2O_3$ | 5.24 | 5.47 | 5.95 | 5.67 | 5.50 |
| CaO | 11.36 | 15.66 | 16.73 | 20.17 | 23.32 |
| MgO | 2.32 | 2.10 | 1.73 | 2.13 | 1.99 |
| $Na_2O$ | 2.18 | 2.16 | 1.91 | 0.85 | 0.85 |
| $K_2O$ | 0.78 | 0.96 | 0.97 | 0.92 | 0.93 |
| $SO_3$ | 2.77 | 2.21 | 3.67 | 1.09 | 1.27 |
| $TiO_2$ | 0.92 | 0.81 | 0.80 | 0.73 | 0.68 |
| BaO | 1.03 | 0.85 | 0.47 | 0.56 | 0.62 |
| MnO | 1.12 | 0.92 | 0.62 | 0.71 | 0.90 |
| $Cl^-$ | 0.58 | 1.11 | 1.59 | 0.45 | 0.40 |
| LOI | 6.54 | 4.48 | 8.45 | 10.92 | 10.91 |
| C /S ratio | 0.28 | 0.35 | 0.37 | 0.49 | 0.55 |
| pH | 10.1 | 12.5 | 12.5 | 11.5 | 11.5 |

gibbsite and CAH gel ($C_3AH_6$; a form of cubic hydrogarnet) of poorly crystalline form; it increases in intensity with hydration ages and C/S ratio. The formation of CSH products with different C/S ratios gave peaks at different temperatures.

According to [27], calcium aluminate hydrates (CAH) significantly affect the specimens' early strength development and setting. On the other hand, increasing the temperature of the endothermic peaks from 70 to 100 °C with increasing the curing age is indicative of the removal of the adsorbed water in the calcium silicate and alumina gel, which is masked by the peak of removal of the hygroscopic water. In all DTA graphs (Figs. 8, 9, 10), as the hydration progresses, CSH and CAH formation results in abroad endothermic peaks, as shown clearly in mixes MD II and MD III. Also, the large amplitude of the endothermic peaks found in 7 days of mixes containing CKD (MD I and MD II) may be due to the holding capacity for water. The broad endothermic peaks that appear at about 500 °C and increase in intensity as hydration age progresses are attributed to the loss of the structural ($OH^-$) from the lattices of the clay minerals.

### 3.5 Physico-mechanical properties of the studied specimens

It is observed that the water absorption for specimens of all mixes that were cured at seven days cannot be determined due to distortion in their geometrical shape (Fig. 11) or disintegration in water at different degrees. Also, all the mixed MD control specimens were disintegrated in water, but the disintegration effect was slightly enhanced after seven days of curing (Fig. 12).

Regarding the bulk density of the stabilized green specimens, it is increased over a period of up to 60 days of curing. MD III specimens (2.15 g/cm$^3$) achieved the highest value at 60 days of moist curing period. Also, specimens of QL addition achieved a dense body comparable to those of CKD addition (Fig. 12).

It is observed that as curing age increases, compressive strength increases (Fig. 12). Moreover, strength increases in proportion to the amount of hydration products formed. The best strength development and the highest compressive strength were recorded for the specimens of MD III stabilized with the GGBS and activated by 5wt.% QL at 60 days (266 kg/cm$^2$), corresponding to 8.5% of water absorption. Moreover, as revealed from all illustrated graphs, the effect of the formation of hydration

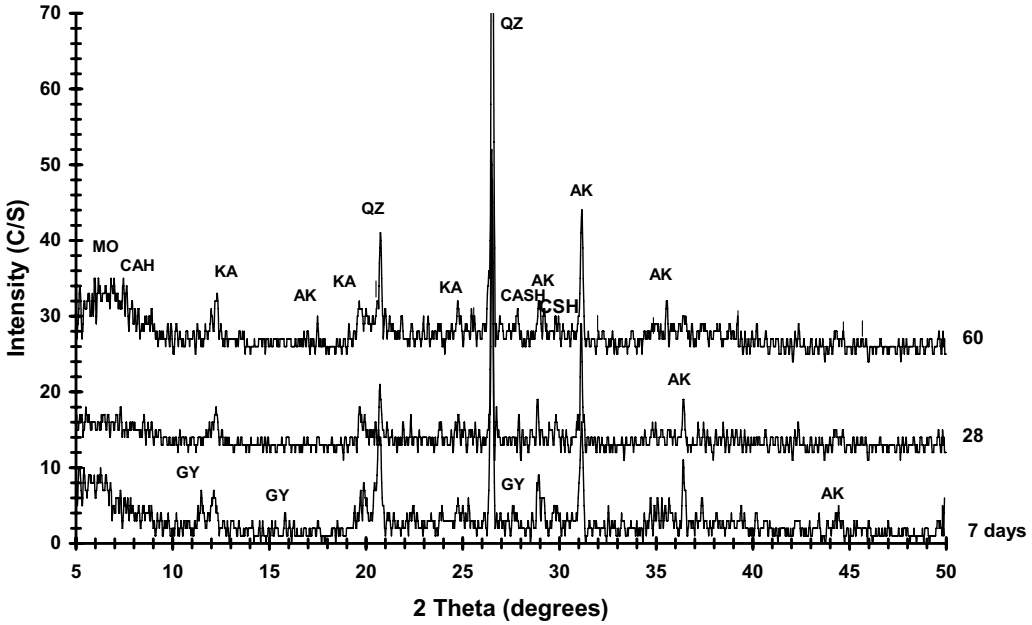


**Fig. 3** XRD patterns of MD control specimens cured for 7, 28, and 60 days. (MO: Montmorillonite, (CSH: Calcium silicate hydrates, CAH: Calcium aluminate hydrates, AK: Akermanite, CASH: Calcium aluminate silicate hydrates, KA: Kaolinite, QZ: Quartz)

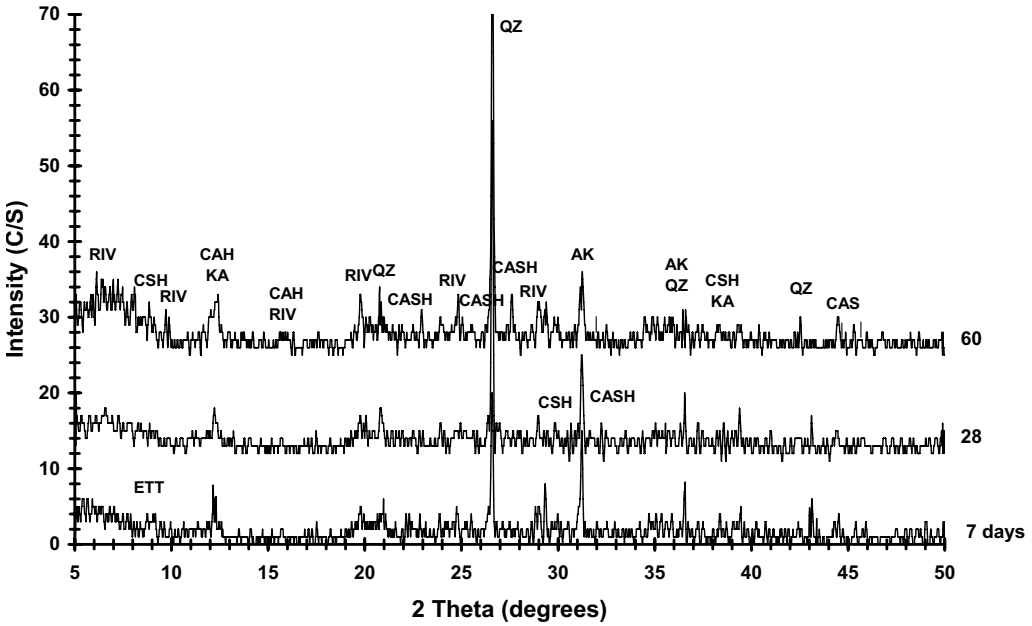


**Fig. 4** XRD patterns of MD I specimens cured for 7, 28, and 60 days (RIV: Riversideite, ETT: Ettringite)

products on the studied properties is obvious after seven days of curing.

On the other hand, the results of the specimen's stability in water show that all specimens of different mixes that were cured for seven days are partially (MD I to MD IV) or completely (MD control) collapsed in water (Table 7). As the curing period progressed ($\geq 14$ days), the mixes of MD I to MD IV specimens can resist the collapsibility effect. On the contrary, specimens of mix MD control can still not resist the water effect even after slightly improving their properties.

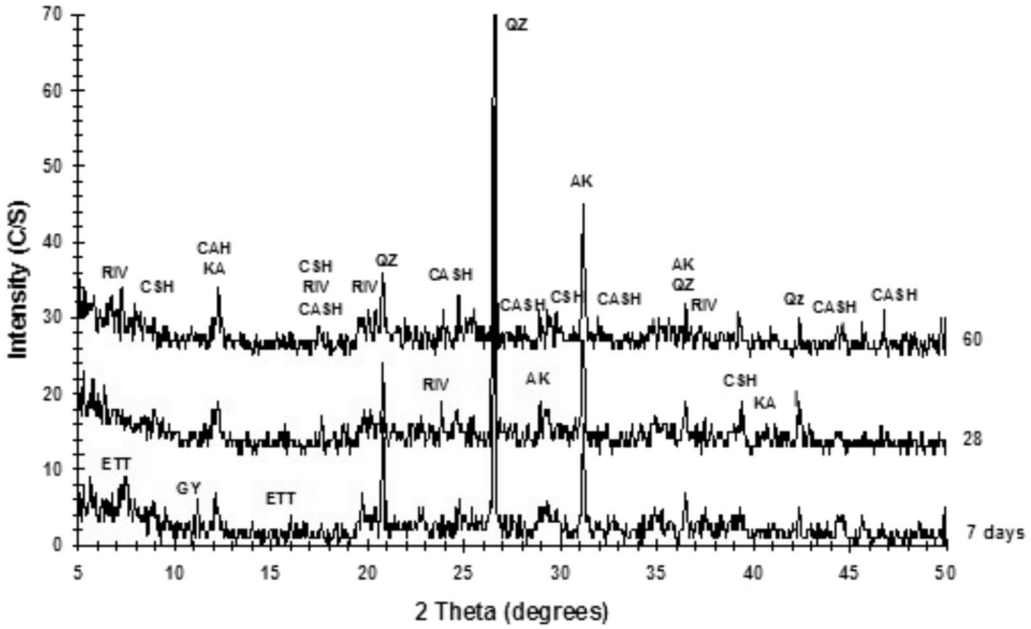


**Fig. 5** XRD patterns of MD II specimens cured for 7, 28, and 60 days. (GY: Gypsum)

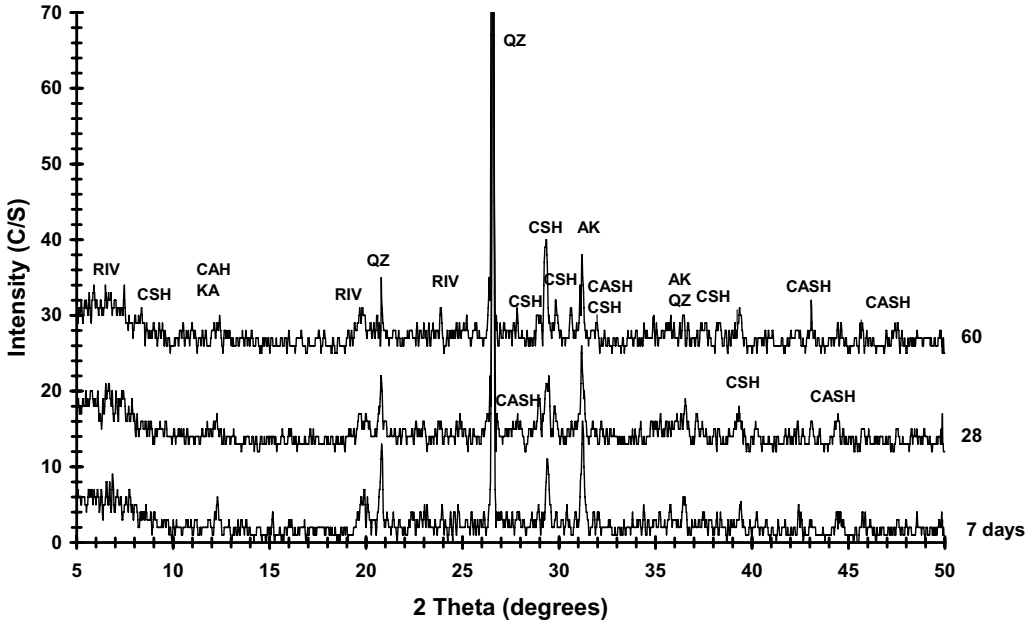


**Fig. 6** XRD patterns of MD III specimens cured for 7, 28, and 60 days

## 4 Discussion

### 4.1 The effect of CKD and QL on the chemical composition of mixes.

It is anticipated from the chemical analysis of mixes that the C/S ratio and high pH value are expected to play an essential role in activating the used slag, pozzolanic activity, formation of hydration, and cementitious products. Adding the CKD to the clay-based mixes raises the pH value to 12.5. This high pH indicates an $OH^-$ ion activity, which is considerably high in CKD mixes, whose pH value is limited to 12.5. According to [28], a high pH value promotes the dissolution of alumina and silica within the specimen.

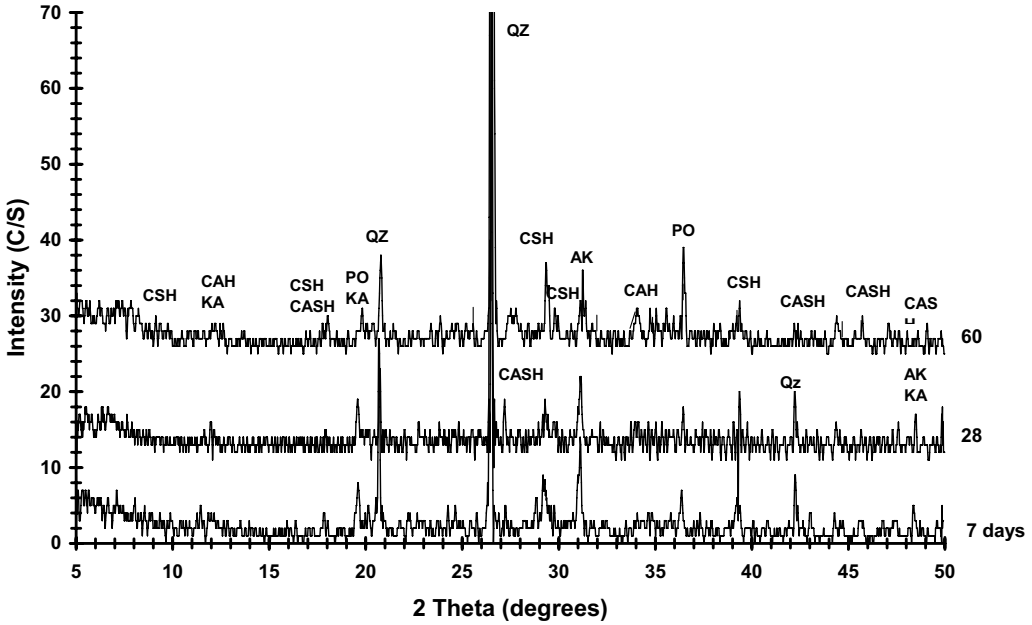


**Fig. 7** XRD patterns of MD IV specimens cured for 7, 28, and 60 days (PO: Portlandite phase)

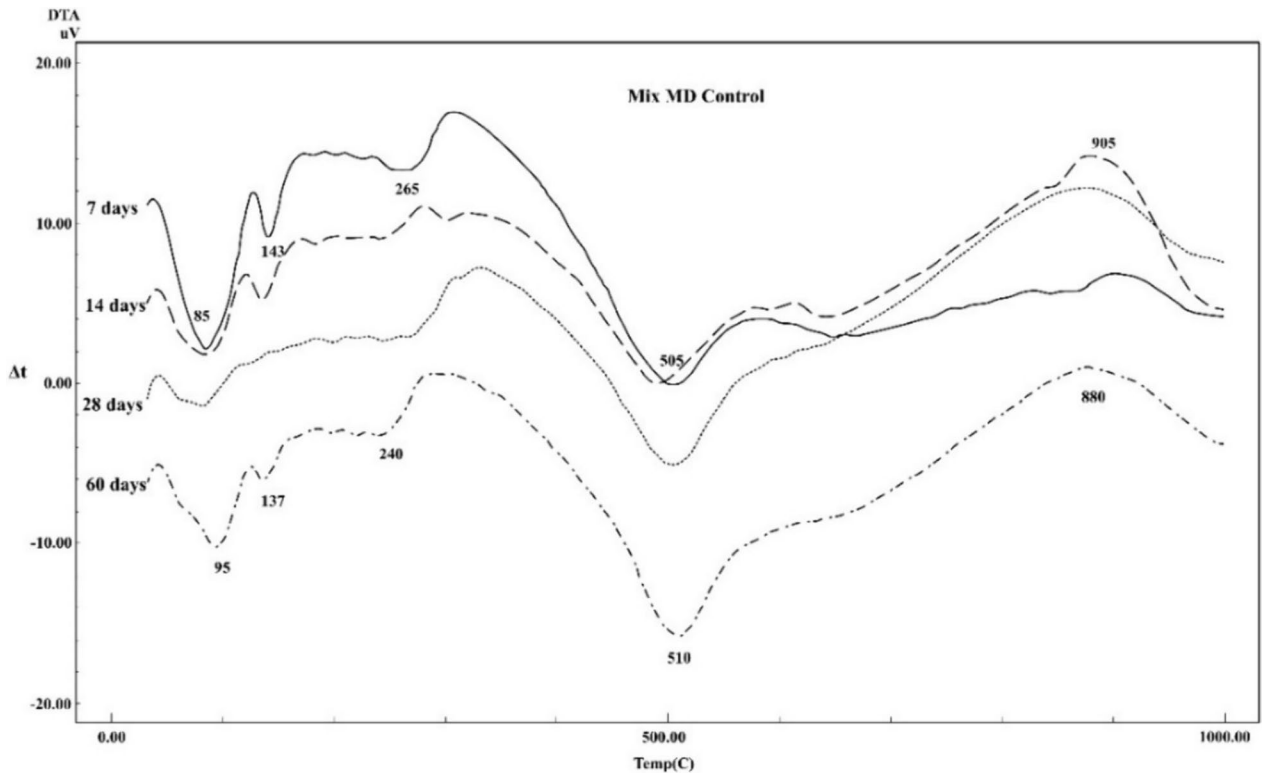


**Fig. 8** Changes in DTA curves of the studied specimen of mix MD control during the curing age and temperature progress

**4.2 The variation in X-ray diffraction analysis of mixes.**

The XRD patterns showed that the hydration products increased with the QL addition rather than the CKD addition as the curing time increased. The reasons for the formation of the CSH and CSAH may be explained as follows:

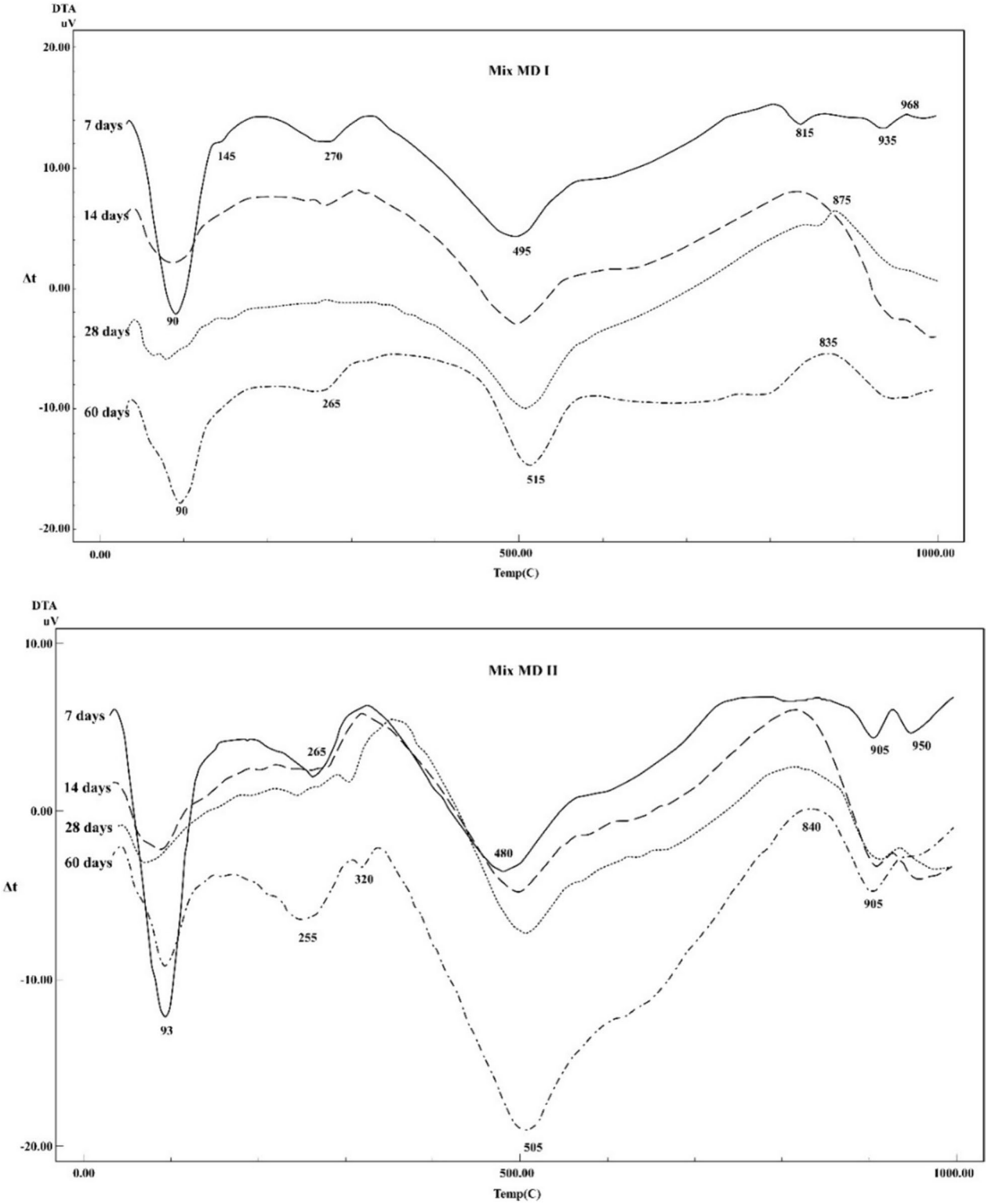


**Fig. 9** Changes in DTA curves of the studied specimens of mixes MD I and MD II during the curing age and temperature progress

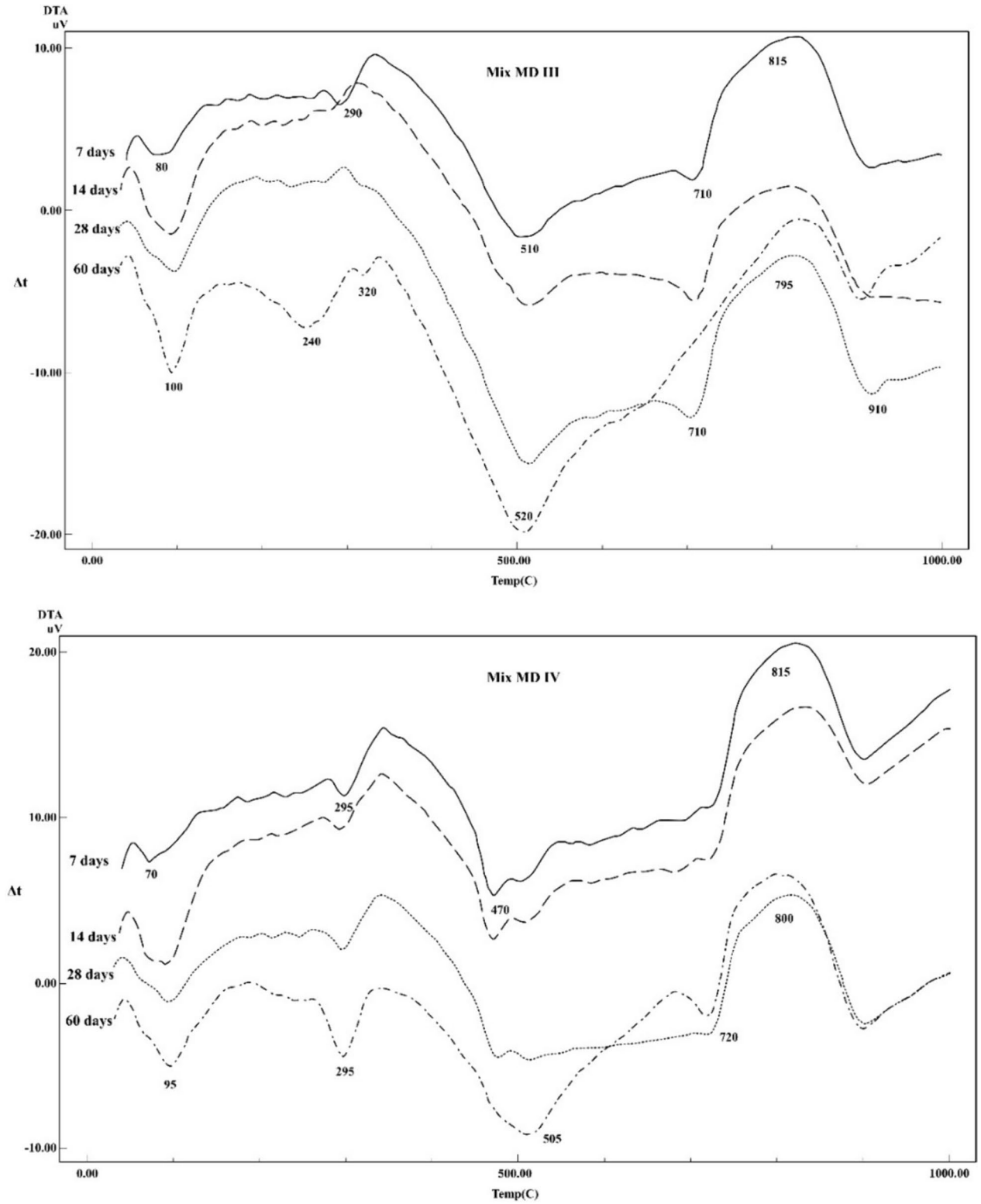


**Fig. 10** Changes in DTA curves of the studied specimens of mixes MD III, and MD IV during the curing age and temperature progress

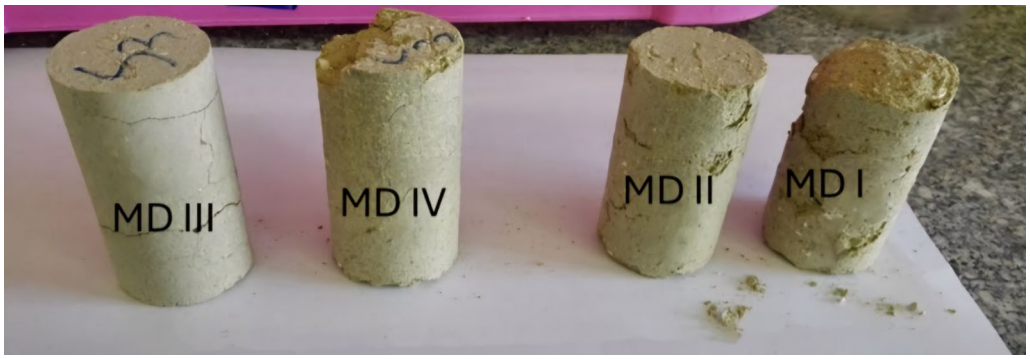


**Fig. 11** Status of the 7 days cured specimens of different mixes after immersion in water for 24 h

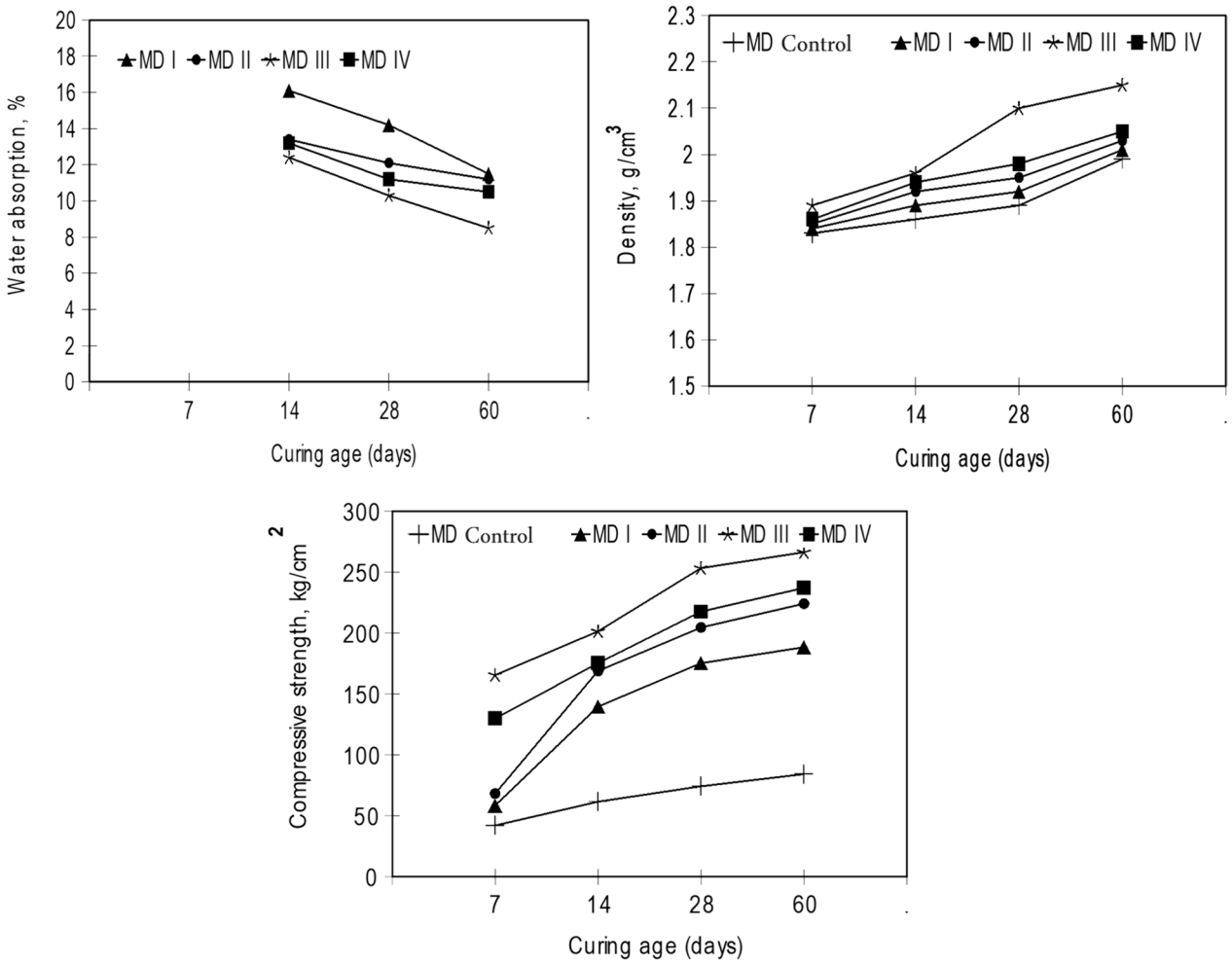


**Fig. 12** Effect of mixes on the properties of their specimens as a function of curing ages

- The used slag belongs to water-cooled blast-furnace slags, which, hydraulically, are very reactive [29]. It contains highly reactive siliceous and aluminous materials in a finely divided form. These materials, in the presence of an alkaline medium (produced by cement, CKD, and QL), will react with the basic components, such as calcium hydroxide released during the hydration of CKD and QL to form com-

**Table 7** Stability of the cured specimens of different mixes toward collapsibility in water

| Specimens of the mix | Specimens cured for (days) | | | |
|---|---|---|---|---|
| | 7 | 14 | 28 | 60 |
| MD control | CC | PC | PC | PC |
| MD I | PC | GD | GD | GD |
| MD II | PC | GD | GD | GD |
| MD III | PC | GD | GD | GD |
| MD IV | PC | GD | GD | GD |

GD : Good, PC: Partially collapsed, CC: Completely collapsed

pounds possessing cementing properties (CSH gel and CASH) [30].

- In addition, GGBS contains CaO, which undergoes a pozzolanic reaction with silica and alumina released from other components (clay and sand), resulting in gel formation [31].

In general, the dispersion of clay minerals is caused by the exchange of metal ions in the clay with calcium ions released from the QL, CKD, and GGBS. This may initiate a process of flocculation that forms a strong agglomeration, preventing water from penetrating and decreasing plasticity[32]. In a slower reaction, aluminates (CASH) and silicates (CSH) complex is formed when calcium chemically reacts with silica and alumina in clay minerals. Many researchers [11, 33] found that the strength and durability behavior of soils were significantly enhanced after the stabilization of soil with calcium-rich material and GGBS. The activation of GGBS in the studied mixes with the presence of moisture and alkaline media causes an increase in gel formation and improves particle binding.

### 4.3 The variation of differential thermal analysis of the mixes.

The variation in the peak's temperature can usually be explained by the variation in the size of the particles and the degree of crystallization. The amplitude of this peak means increasing the amount of the removable $OH^-$ group with curing time. This marks the dissolution of the added slag and its reactivity in the alkaline medium. Hence, when lime-rich material is added, the alkaline media releases $Ca^{2+}$ and Al $(OH)^{4-}$ ions from the slag [27]. Within the same temperature range, it is partly possible to interface between the loss of the structural ($OH^-$) and the final stage of dehydration of CSH and hydrated aluminate phases.

Generally, the activating slags typically yield products whose properties are close to those of normal Portland cement pastes. The small endothermic peak detected only in the thermographs of the mix MD IV at about 470 °C could be attributed to the dehydration of calcium hydroxide (portlandite) formed from the hydration of access-free lime (10wt.% QL) present in this mix. So, the formation of portlandite resulted in a low specimen strength compared to mix MDIII (5wt.% QL). Additionally, the DTA curves of the mixes MD III and MD IV exhibited a small endothermic peak at about 700 °C, which is probably associated with the de-carbonation of calcium carbonate. In normal hydration settings, it is not easy to prevent the lime from carbonating when it comes into contact with air. The sulfate contained in the mix MD control may dissolve in the alkaline media and, after a certain period (7 days), cause gypsum to precipitate. As gypsum is gradually consumed, the CSH and CAH start to form. The cement and gypsum content may activate the slag, which could result in the formation of CAH, but it cannot influence the activation of the GGBS added. The exothermic distinct peaks shown at about 800 °C were found evidently in mixes MD I, MD II, MD III, and MD IV, and approximately in the mix MD control denote the devitrification effect of the GGBS. The temperature, the number, and the intensity of the peaks differ from one slag to the other. Based on the DTA results, it can be concluded that the specimen's strength will increase with curing ages due to the hydration products formed in the clay-OPC-lime-slag and clay-OPC-cement kiln dust-slag mixes.

Furthermore, the amplitude of the endothermic effects in mixes MD III and MD II at about 250 and 300 °C show the largest endothermic peaks comparable to the other mixes at the same temperatures. Also, the peak intensity of the endothermal and exothermal effects in mix MD control (contains no CKD and QL) are the lowest amplitude comparable to the peaks of the other mixes, particularly the hydration products.

### 4.4 The effect of CKD and QL on the physico-mechanical properties of the lab-made specimens.

The specimens of all mixtures cured at seven days exhibited shape distortion or disintegration at varying degrees in the water, making it impossible to quantify the water absorption. The reason for this effect is that the quantity of the hydration binding products that started to form at the early stage is insufficient but developed later, from day 14 up to 60 days. The results of the XRD and DTA analyses confirmed this result. Also, all the MD control specimens were disintegrated in water at the early curing times, but the disintegration effect was slightly enhanced after seven days of curing. This is because there are not enough significant amounts of cementing products; therefore, the addition of GGBS with weak activators did

not show a considerable increase in strength development even with curing periods increased. However, the mix MD control may have activated GGBS with some minerals present in the KHC, such as gypsum and the added OPC.

The hydration of GGBS is improved by the sulfate found in the gypsum mineral in KHC. Similar sulfate activation for GGBS has already been noted [34]. The water absorption results indicated that when the QL dosage decreased, and the CKD dosage increased, the amount of water absorbed reduced, demonstrating that the calcite and portlandite phases (as identified by the XRD and DTA) played a negative substantial effect in the impermeability of the examined specimens, but the formation of the hydration products (such as CSH and CAH) played a positive role. It achieved the highest absorption value in MD I (5wt.% CKD) cured at 14 days and the best value (8.5%) in MD III specimens (5wt.%QL) cured for 60 days. In general, the addition of QL and CKD encouraged the formation of CSH, which serves as a cementing agent, binding the clay particles together and giving the clay body strength [32, 35, 36].

Additionally, as curing time increased, water absorption was reduced for all specimens. This is explained by the fact that all XRD patterns showed the production of the effective CSH during a prolonged curing period (at least 14 days) as a crystalline hydrated state. This outcome is consistent with the results of other researchers [37]. When CSH is produced and accumulated, it results in the closure of some open pores, which reduces their capacity to absorb water.

The increase in bulk density is due to the produced phases filling the void spaces and joining the components in the specimens. As a result, the MD III specimens with the highest hydration phase content (as identified by the XRD and DTA) have the highest bulk density.

It is worth mentioning that the production of pozzolanic reaction products that fill the pores in studied mixes may make the specimens dense and increase the compressive strength. The activated GGBS advances the role of the added GGBS by gradually forming insoluble calcium silicate hydrate and calcium aluminate hydrate compounds as cementing products that serve as binders and reinforce the specimen body through its pozzolanic reaction with calcium hydroxide in the presence of water. Moreover, more additions of the quicklime may encounter some difficulties in continuing its real role. The $Ca^{2+}$ is more than needed, leading to the formation of portlandite (which has no cementitious character) and encouraging calcite formation with the $CO_2$ from the air, negatively affecting the engineering properties [38]. Also, as the curing age progresses, the hydration products, especially the portlandite phase (CaOH), may cover parts of the clay particles. These stages may leave an impervious, insoluble layer on the clay particles. This might be the cause of lower strength values.

The development of the cementitious phases with the curing time is the primary cause of the stability of the stabilized specimens in water. When the activator is added to GGBS, the studied mixes with high silica and alumina levels produce considerably more complex hydrates (CSH and CAH). The rate of this hydration reaction is slower than with Portland cement. It acts as a pore-blocker, increasing the clay-based specimens' long-term hardness and resistance to water collapsibility.

Finally, the stabilized green specimens of mixes MD I to MD IV cured for 14 days or more exhibited good physical and mechanical behavior concerning water absorption, bulk density, compressive strength properties, and resistivity to water collapsibility. Also, mix MD III (clay-OPC-5wt.% QL-GGBS) had superior properties, followed by MD IV (clay-OPC-10% QL-GGBS), then MD II (clay-OPC-10% CKD-GGBS), then MD I (clay-OPC-5% CKD-GGBS) and the latest is the mix of MD control (clay-OPC-GGBS). Hence, all the activated studied specimens can be used successfully as building units based on the physico-mechanical test results. Consequently, the waste used can be shared for useful applications in the construction field. Finally, it was concluded that the bricks made of optimum cement kiln dust (CKD) and quick lime (QL) could be utilized in masonry construction as it fulfilled the criteria of different compressed earth classes in terms of dry compressive strength (30–70 $kg/cm^2$), water absorption (8–15%) and density (1.7–2 $gm/cm^3$) per the Egyptian standard specifications for the building by compressed Earth blocks [22].

## 5 Conclusion

Based on the findings and analyses presented in this paper, it was observed that the engineering properties of the specimens were significantly affected by the formation of hydration products. The curing age and the C/S ratio are directly proportional to the amount and quality of the hydration products formed. To achieve good engineering properties and ensure good performance in the activation and stabilization processes, it is recommended that the specimens containing QL and CKD must be cured for at least 14 days. QL and CKD act as alkaline activators for the GGBS. Mixes containing quicklime specimens had superior properties in comparison to those with cement kiln dust. However, using more than 5% of QL is not desired. Although the 14-day cured specimens containing CKD and QL showed resistance against collapsibility in water, it is still important to take precautions against excessive humidity and extended wetness. Increasing amounts of CKD in the mixtures result in better characteristics. The use of CKD and GGBS to

manufacture stabilized green bricks leads to a reduction in the negative impacts of industrial wastes.

**Abbreviations**

| | |
|---|---|
| GGBS | Ground granulated blast-furnace steel slag |
| CKD | Cement kiln dust |
| Ql | Quicklime |
| DTA | Differential thermal analysis |
| XRF | X-ray fluorescence |
| XRD | X-ray diffraction |
| CAH | Calcium aluminate hydrates |
| CASH | Calcium aluminate silicate hydrates |
| CSH | Calcium silicate hydrates |
| KHC | Kafr Homied clay |
| OPC | Ordinary Portland cement |
| QZ | Quartz |
| I | Illite |
| AK | Akermanite |
| LI | Lime |
| CA | Calcite |
| LA | Larnite |
| SY | Sylvite |
| BR | Brownmillerite |
| CS | Calcium silicate |
| MO | Montmorillonite |
| KA | Kaolinite |
| RIV | Riversideite |
| ETT | Ettringite |
| GY | Gypsum |
| PO | Portlandite |

**Acknowledgements**
The authors would like to thank Dr Ahmed Abou Bakr Omar, Housing and Building National Research Center, Cairo, Egypt, for his support in the present work

**Author contributions**
All authors contributed to the study's conception and design. Material preparation, data collection, and analysis were performed by MSE-M and SAM. The first draft of the manuscript was written by MSE-M. SAM commented on previous versions of the manuscript. All authors read and approved the final manuscript.

**Funding**
No funding was received to assist with the preparation of this manuscript.

**Availability of data and materials**
All data analyzed during this study are included in this published article.

## Declarations

**Ethics approval and consent to participate**
Not applicable.

**Consent for publication**
Not applicable.

**Competing interests**
The authors declare that there is no competing interests.

Received: 9 January 2024 Accepted: 6 June 2024
Published online: 14 June 2024

**References**

1. Ahmed HM, Hefni MA, Ahmed HA, Saleem HA (2023) Cement kiln dust (CKD) as a partial substitute for cement in pozzolanic concrete blocks. Buildings 13(2):568:1-619. https://doi.org/10.3390/buildings13020568
2. Almuaythir S, Abbas M (2023) Expansive soil remediation using cement kiln dust as stabilizer. Case Stud Constr Mater 18(e01983):1–14. https://doi.org/10.1016/j.cscm.2023.e01983
3. Mebarkia R, Bouzeroura M, Chelouah N (2022) Study of the effect of cement kiln dust on the mechanical, thermal and durability properties of compressed earth blocks. Constr Build Mater 349(128707):1–14. https://doi.org/10.1016/j.conbuildmat.2022.128707
4. Bagheri SM, Koushkbaghi M, Mohseni E, Koushkbaghi S, Tahmouresi B (2020) Evaluation of environment and economy viable recycling cement kiln dust for use in green concrete. J Build Eng 32:101809. https://doi.org/10.1016/j.jobe.2020.101809
5. Sreekrishnavilasam A, Rahardja S, Kmetz R, Santagata M (2007) Soil treatment using fresh and landfilled cement kiln dust. J Construct Build Mater 21(2):318–327. https://doi.org/10.1016/j.conbuildmat.2005.08.015
6. Peethamparan S, Olek J, Diamond S (2009) Mechanism of stabilization of Na-montmorillonite clay with cement kiln dust. J Cement Concr 39(7):580–589. https://doi.org/10.1016/j.cemconres.2009.03.013
7. Yadu L, Tripathi RK (2013) Effects of granulated blast furnace slag in the engineering behaviour of stabilized soft soil. Procedia Eng 51:125–131. https://doi.org/10.1016/j.proeng.2013.01.019
8. Kogbara RB, Al-Tabbaa A (2011) Mechanical and leaching behaviour of slag-cement and lime-activated slag stabilized/ solidified contaminated soil. J Sci Total Environ 409(11):2325–2335. https://doi.org/10.1016/j.scitotenv.2011.02.037
9. Higgins DD (2005) Soil stabilization with ground granulated blast furnace slag. Cementitious Slag Makers Association (CSMA), London
10. Obuzor GN, Kinuthia JM, Robinson RB (2011) Utilization of lime activated GGBS to reduce the deleterious effect of flooding on stabilized road structural materials: a laboratory simulation. J Eng Geol 122(3–4):334–338. https://doi.org/10.1016/j.enggeo.2011.06.010
11. Oti JE, Kinuthia JM, Bai J (2009) Compressive strength and microstructural analysis of unfired clay masonry bricks. Eng Geol 109(3–4):230–240. https://doi.org/10.1016/j.enggeo.2009.08.010
12. Ni H, Wu W, Lv S, Wang X, Tang W (2021) Formulation of non-fired bricks made from secondary aluminum ash. Coatings 12(1):2. https://doi.org/10.3390/coatings12010002
13. Zhang J, Srinivasan RS, Peng C (2020) Ecological assessment of clay brick manufacturing in china using emergy analysis. Buildings 10(11):190. https://doi.org/10.3390/buildings10110190
14. The Bangladesh Gazette (2013) The brick manufacturing and brick kilns establishment (Control) Act. Government of Bangladesh, Dhaka
15. Asif HA, Akhter HS (2019) Role of laws to control brick manufacturing and kiln establishment in Bangladesh Scope of alternative bricks. VNU J Sci Earth Environ Sci. https://doi.org/10.25073/2588-1094/vnuees.4371
16. Boussaa N, Kheloui F, Chelouah N (2023) Mechanical, thermal and durability investigation of compressed earth bricks stabilized with wood biomass ash. Constr Build Mater 364:129874. https://doi.org/10.1016/j.conbuildmat.2022.129874
17. Shourijeh PT, Rad AM, Bigloo FH (2022) Application of recycled concrete aggregates for stabilization of clay reinforced with recycled tire polymer fibers and glass fibers. Constr Build Mater 355:129172. https://doi.org/10.1016/j.conbuildmat.2022.129172
18. Wang W, Gan Y, Kang X (2021) Synthesis and characterization of sustainable eco-friendly unburned bricks from slate tailings. J Mater Res Technol 14:1697–1708. https://doi.org/10.1016/j.jmrt.2021.07.071
19. BS EN.: Cement-Part (1) (2000) Composition, specification and conforming criteria for common cements. 197-1: 1–38.
20. ASTM D4972-19 (2019) Standard test method for pH of soils. Standard Annual Book of ASTM, 4, 08
21. Engbert A, Plank J (2020) Impact of sand and filler materials on the hydration behavior of calcium aluminate cement. J Am Ceram Soc 104(5):1067–1075. https://doi.org/10.1111/jace.17505
22. Egyptian Code for the Building by the Soil (ECBS) )2016( The building by the stabilized and compressed earth blocks. 1, 1–144.
23. Egyptian Standard Specification (2008) Quick and hydrated lime- Part (1): Definitions, requirements and conformity criteria. Egypt: 584–1.

24. Khater HM (2012) Effect of cement kiln dust on geopolymer composition and its resistance to sulfate attack. Green Mater 1(1):36–46. https://doi.org/10.1680/gmat.12.00003
25. El-Mahllawy MS, Kandeel AM (2014) Engineering and mineralogical characteristics of stabilized unfired montmorillonitic clay bricks. J HBRC 10(1):82–91. https://doi.org/10.1016/j.hbrcj.2013.08.009
26. Ramachandran VS, Paroli RM, Beaudoin JJ, Delgado AH (2002) Handbook of thermal analysis of construction materials. Noyes and William Andrew Publishing, New York
27. Doneliene J, Eisinas A, Baltakys K, Bankauskaite A (2016) The effect of synthetic hydrated calcium aluminate additive on the hydration properties of OPC. Adv Mater Sci Eng 2:1–8. https://doi.org/10.1155/2016/3605845
28. Bagheri M, Lothenbach B, Shakoorioskooie M, Scrivener K (2022) Effect of different ions on dissolution rates of silica and feldspars at high pH. J Cement Concr Res 152:106644. https://doi.org/10.1016/j.cemconres.2021.106644
29. Mostafa NY, El-Hemaly SA, Al-Wakeel EI, El-Korashy SA, Brown PW (2001) Characterization and evaluation of the hydraulic activity of water-cooled slag and air-cooled slag. Cem Concr Res 31(6):899–904. https://doi.org/10.1016/S0008-8846(01)00497-5
30. Amin AM, Ebied E, El-Didamony H (1995) Activation of granulated slag with calcined cement kiln dust. Silic Ind 60(3–4):109–115
31. Keramatikerman M, Chegenizadeh A, Nikraz H (2016) Effect of GGBFS and lime binders on the engineering properties of clay. Appl Clay Sci 132:722–730. https://doi.org/10.1016/j.clay.2016.08.029
32. Sekhar DC, Nayak S (2018) Utilization of granulated blast furnace slag and cement in the manufacture of compressed stabilized earth blocks. Constr Build Mater 166:531–536. https://doi.org/10.1016/j.conbuildmat.2018.01.125
33. Kinuthia JM, Wild S, Jones G (1999) Effects of monovalent and divalent metal sulphates on consistency and compaction of lime- stabilized. Appl Clay Sci 14(1–3):27–45. https://doi.org/10.1016/S0169-1317(98)00046-5
34. Wild S, Kinuthia JM, Robinson RB, Humphreys I (1996) Effects of ground granulated blast furnace slag (GGBS) on the strength and swelling properties of lime-stabilized kaolinite in the presence of sulphates. Clay Miner 31(3):423–433. https://doi.org/10.1180/claymin.1996.031.3.12
35. Muntohar AS (2011) Engineering characteristics of the compressed-stabilized earth brick. Construct Build Mater 25(11):4215–4220. https://doi.org/10.1016/j.conbuildmat.2011.04.061
36. Alavéz-Ramírez R, Montes-García P, Martínez-Reyes J, Altamirano-Juárez DC, Gochi-Ponce Y (2012) The use of sugarcane bagasse ash and lime to improve the durability and mechanical properties of compacted soil blocks. Constr Build Mater 34:296–305. https://doi.org/10.1016/j.conbuildmat.2012.02.072
37. James J, Rao S (1986) Reaction product of lime and silica from rice husk ash. Cem Concr Res 16(1):67–73. https://doi.org/10.1016/0008-8846(86)90069-4
38. Millogo Y, Hajjaji M, Ouedraogo R (2008) Microstructure and physical properties of lime-clayey adobe bricks. Constr Build Mater 22(12):2386–2392. https://doi.org/10.1016/j.conbuildmat.2007.09.002


## Publisher's Note